Article

J. Mex. Chem. Soc. **2007**, *51(2),* 72-80

ISSN 1870-249X

Synthesis and Characterization of Multilayer Films of Dendrimer-Assembled C_{60} Materials on Nanocrystalline TiO_2 Electrodes

Erika Bustos Bustos,[1] Juan Manríquez Rocha,[1] Luis Echegoyen,[2] Thomas W. Chapman[1] and Luis A. Godínez*[1]

[1] Electrochemistry Department, Centro de Investigación y Desarrollo Tecnológico en Electroquímica S.C., P.O. Box 064, C.P. 76700, Pedro Escobedo, Querétaro, México. Phone: 52-442-211-6006, Fax: 52-442-211-6007 lgodinez@cideteq.mx
[2] Department of Chemistry, Clemson University, Clemson, SC-29634, USA.

Recibido el 24 de agosto de 2006; aceptado el 9 de febrero de 2007

Abstract: Nanocrystalline TiO_2 electrodes were silanized and further modified with C_{60} fullerene films linked by Starburst™ (PAMAM G0.0) dendrimers of poly(amidoamine), generation 0.0, using a layer-by-layer technique into either branched dendritic or linear structures. The resulting films provide organized nanoassembled photoactive surfaces that adsorb in the visible region and offer a high molar extinction coefficient. The linear nanocomposite structure in particular increases the photocurrent efficiency of the polycrystalline TiO_2 and decreases the recombination effect, yielding a global collection efficiency of 0.14%.
Keywords: Modified electrodes, fullerene C_{60}, dendrimers, TiO_2, silanized, photovoltaic cells.

Resumen: Electrodos nanocristalinos semiconductores de TiO_2 fueron silanizados y modificados con películas de fulereno C_{60} y dendrímeros de poli(amidoamina) generación 0.0 (PAMAM G0.0), usando la técnica de capa-por-capa en una secuencia dendrítica y lineal. Las películas resultantes proporcionan superficies nanoensambladas fotoactivas organizadas que, además de absorber en la región visible, presentan altos coeficientes de extinción molar. En particular, la organización lineal incrementó la eficiencia de fotocorriente del TiO_2 policristalino minimizando el efecto de recombinación, con lo que se alcanzó una eficiencia de colección global del 0.14%.
Palabras clave: Electrodos modificados, fulereno C_{60}, dendrímeros, TiO_2, silanizado, celdas fotovoltáicas.

Introduction

One of the more promising devices for chemistry-based solar-energy conversion (light-to-electricity) is the semiconductor / liquid junction solar cell. The principle of such devices involves direct collection of light by the semiconductor, where the requirement for light collection is that the incident photonic energy exceeds the gap in energy between the valence and the conduction bands of the semiconductor. The direct-energy-conversion strategy clearly is best suited to semiconductor materials that can absorb significant portions of the solar spectrum, that is, materials with bandgaps of ca. 1 to 2 eV. Unfortunately, many materials with acceptable bandgaps are susceptible to destructive hole-based reactions. Other candidate materials based on metal oxides typically are chemically stable and kinetically resistant to photocorrosion under photoconversion conditions but exhibit bandgaps too large to permit significant collection of visible light (i.e., light of 400 – 700 nm wavelength). For example, the bandgap, ε_g, for the anatase phase of TiO_2 is 3.2 eV, yielding an absorption onset below 400 nm (ca. 380 nm). Wide-bandgap semiconductors can, however, be converted into visible-light absorbers by coating them with light-absorbing dye molecules [1-3]. For this purpose, the surface of a semiconductor material can be covered with a monolayer of a carefully chosen visible-light-harvesting compound, promoting selective injection of photogenerated electrons directly into the conduction band of the semiconductor substrate. At the same time, the dye may mediate the coupled oxidation of a redox carrier in the electrolytic solution. If so, sensitized nanocrystalline semiconductor (NSc) electrodes, characterized by large roughness factors, can be used to assemble devices that work in a regenerative continuous fashion with visible light and provide efficiencies comparable to those obtained in solid-state silicon-based solar cells [3].

Fullerene C_{60} appears attractive as a dye of choice because its absorption spectrum closely matches the requirements of practical photovoltaic devices [4], whether the application be with the solar spectrum for energy conversion or with artificial light sources for indoor use. It offers a high optical absorption coefficient across the visible spectrum with rapid excitation and relatively slow subsequent relaxation [5]. Unfortunately, most published reports indicate only weak photoelectrochemical activity of thin fullerene films under visible-light excitation. A major problem in these studies has been the inability to cast thin fullerene films that can efficiently absorb most of the incident light. Some of the common deposition methods include spin coating, thermal evaporation casting of Langmuir-Blodgett films, and self-assembly of monolayer films on gold surfaces [6]. The latter methods produce the most organized surfaces [7] but with the inconvenience of poor mechanical stability [8]. Multilayers of C_{60} have been produced in a stepwise fashion via self-assembly [9-10]. The resulting films, produced by a multilayered covalent surface-modification method, exhibited interesting mechanical, electrical, electrochemical, and optical properties. On the other hand, this method yields relatively disorganized, thick films, which promote the undesirable recombination reaction. To solve this problem, we seek to produce more highly organized C_{60} multilayer films on a semiconductor by means of dendrimer linkages. Dendrimer molecules are geometrically regular hyperbranched species, similar to covalent

micelles, that have been used successfully to modify electrode surfaces and to control the molecular architecture that forms at the electrode-solution interface [11].

The purpose of this paper is to describe the construction of stable photocatalytic fullerene clusters over silane-modified NSc TiO_2 electrodes. Electrode surfaces were coated layer-by-layer with C_{60} fullerene linked by Starburst™ G0.0 PAMAM dendrimers in either a linear (Fig. 1A) or dendritic (Fig. 1B) sequence. The resulting nanoassembled surface films, each with a distinct structure, both absorb in the visible region and present higher molar extinction coefficients than self-assembled films of C_{60}, increasing the photocurrent efficiency compared with that reported in the literature. They also retard the parasitic recombination reaction.

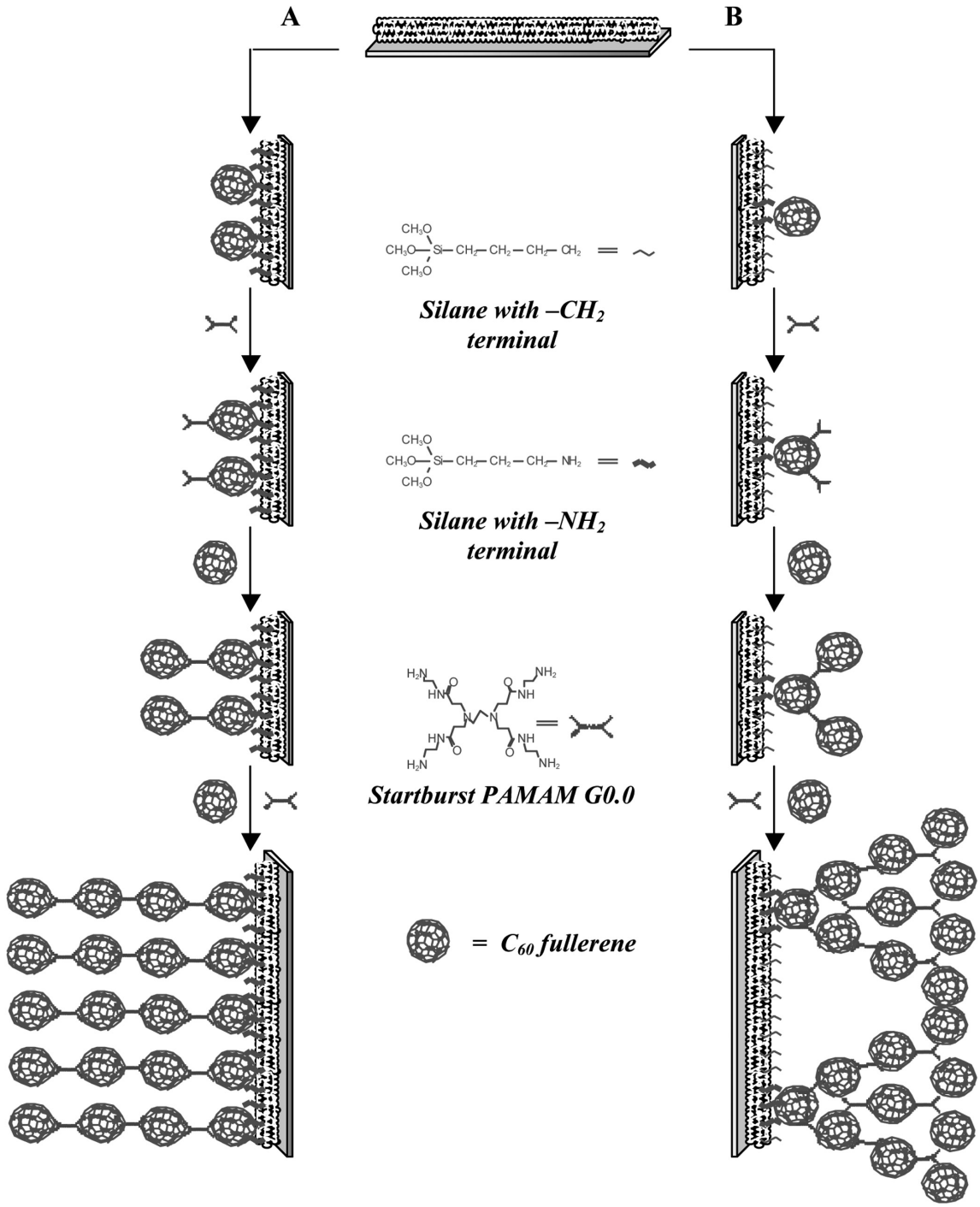

Fig. 1. Schematic representation of NSc TiO_2 electrodes modified with silanes, C_{60} fullerene and Startburst PAMAM G0.0 by the: (**A**) linear and (**B**) dendritic sequence procedures.

Results and Discussion

NSc TiO_2 electrodes were prepared by electrophoretic deposition of the colloidal titanium oxide on ITO-coated conducting-glass substrates [12], yielding roughness factors of 540 and an average thickness value of 15 mm [13]. These surfaces were characterized by XRD (Fig. 2), where we find the anatase phase of TiO_2 at 25° of the 2θ signal with [1,0,1] crystallographic orientation. The TiO_2 flat-band potential observed for these oxide films (E_{FB}, -0.2V *vs* NHE) was significantly smaller than that reported previously (-0.5V *vs* NHE) [13-14].

The NSc TiO_2 electrodes were then coated with the fullerene films through silane linkages. To produce dendritic films, solutions containing 3% $(CH_3O)_3Si(CH_2)_3NH_2$ + 3% $(CH_3O)_3Si(CH_2)_3CH_2$ were used to provide sufficient spacing between the aminated silane links on the surface for branched structures to develop. Linear fullerene structures were obtained by using only 3% $(CH_3O)_3Si(CH_2)_3NH_2$ in the surface preparation. After the chemical pre-treatment [15] the presence of cross-linked polysiloxane was verified with FT-IR spectroscopy [16], as the asymmetric stretching and bending of –Si-O-Si- vibration between 1040 and 1200 cm^{-1} and the C-H stretching bands of the alkyl chain of the silane between 2800 and 2940 cm^{-1} were observed (Fig. 3). In addition, these surfaces were inspected by mapping SEM microscopy (Fig. 4), which confirmed good homogeneity of Ti and Si coverage for both pretreatments.

In order to determine the reaction time required to form the most efficient fullerene films on the NSc TiO_2 surfaces, the NSc TiO_2 electrodes silanized with 3% $(CH_3O)_3Si(CH_2)_3NH_2$ were treated with a 0.67 mM C_{60} fullerene solution containing 1.33 mM PAMAM G0.0 in 2:1 V/V CH_2Cl_2 /toluene at 323 K. The N-H nucleophilic addition reaction of the primary amines of the silane or dendrimer across one of the C=C bonds in C_{60} fuses two six-membered rings to the silane or to subsequent dendrimer links. This reaction was carried out under reflux in order to permit the self-assembly of a covalently bound fullerene layer [10, 17]. The times of reaction were set at 2, 4, 6, 9 or 16 hours. The resulting electrodes modified by a layer of fullerene for each reaction time were tested in photovoltaic experiments at 430 nm, which corresponds to the fullerene moiety absorbance wavelength [4, 18].

From these tests the highest values of the Incident Photon-to-Current Efficiency (IPCE, monochromatic efficiency at 430 nm) and of the Energy Conversion Efficiency (η, polychromatic efficiency) were obtained for 9 h of reaction (58 % and 0.00024 %, respectively; Fig. 5 and Table 1). Nine hours of fullerene-binding reaction also produced FT-IR spectra with the strongest carbon signals as well as the greatest electronic transferences in cyclic voltammetry (data not shown), corroborating that the IPCE % has a direct relationship with the quantity of carbon on the surface. Consequently, this reaction time was used in each subsequent step during the construction of the multilayer nanoassembled electrodes, which were formed layer-by-layer in four sequential steps of fullerene–PAMAM-dendrimer treatment to organize the surface. In the case of the

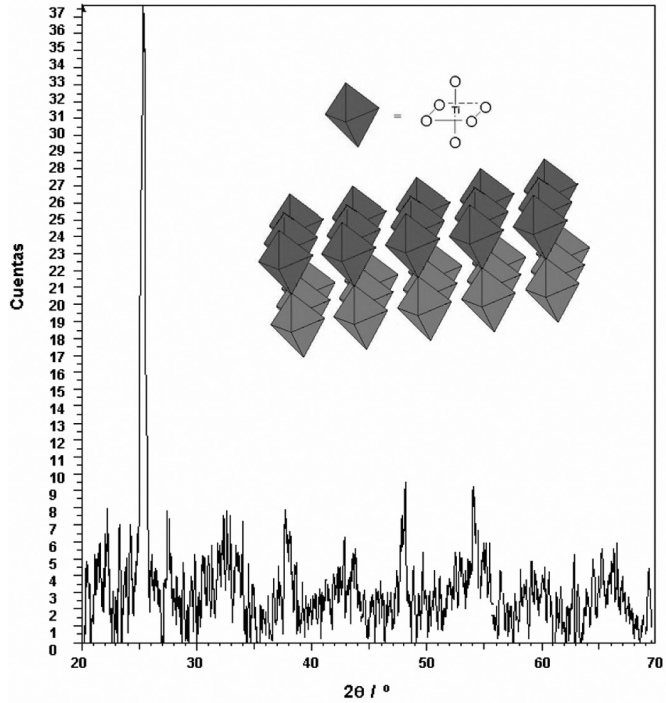

Fig. 2 XRD of NSc TiO_2 anatase phase at 298 K between 2θ of 20° and 80° with a step size of 0.2°, rotating sample.

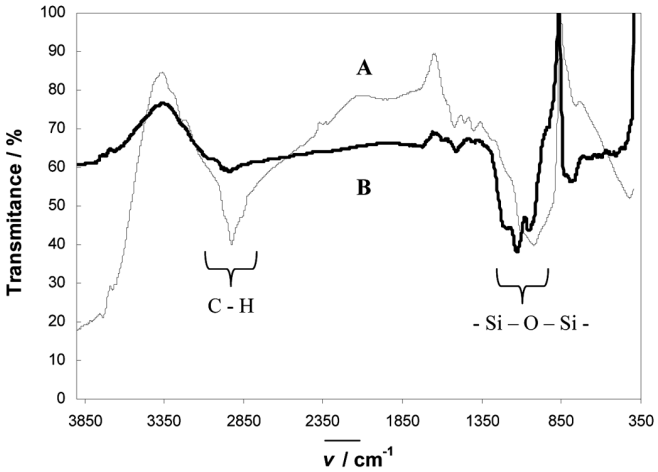

Fig. 3. FT-IR spectrum of NSc TiO_2 silanized with (**A**) 3% $(CH_3O)_3Si(CH_2)_3NH_2$ + 3% $(CH_3O)_3Si(CH_2)_3CH_2$ and (**B**) 3% $(CH_3O)_3Si(CH_2)_3NH_2$. Data taken with 250 scans at 45° reflection angle at 298 K, using as reference the spectrum of NSc TiO_2.

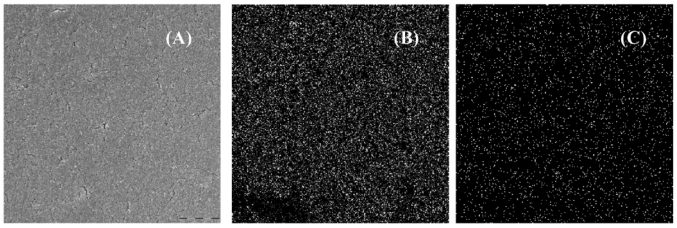

Fig. 4. SEM image of (**A**) silanized NSc TiO_2 and mapping of (**B**) Ti and (**C**) Si over the same sample at 2000X with 14 kV acceleration voltage.

linear fullerene addition method, the concentration of dendrimer exposed to the surface prior to each step of fullerene addition was held constant at 1 mM to produce the modified electrodes represented in Fig. 1A. For the dendritic films, the concentration of PAMAM G0.0 in the dendrimer solution was increased geometrically prior to each step of fullerene addition (i.e., from 0.1 to 1 to 10 mM PAMAM before steps 2, 3 and 4, respectively) to support the branching structure represented schematically in Fig. 1B. Toluene at 363 K and CH_2Cl_2 at 323 K were used as solvents in the C_{60} and PAMAM modification steps, respectively.

The presence of fullerene on the silanized NSc TiO_2 was confirmed by the FT-IR spectra for both methods of electrode preparation. In Figure 6A it is seen that there are strong fullerene signals for both modification methods, appearing at all of the various frequencies in the C_{60} skeleton ring vibration region between 1050 and 1750 cm^{-1} [9, 19-22]. According to the literature [8, 10], the bonding between C_{60} units and primary amines occurs through nucleophilic addition of the amines onto the C_{60} molecules. This was verified by means of FT-IR experiments in which a signal related to the –N-C- stretching vibration of the dendrimers was identified at 3250-3600 cm^{-1} [9, 19-20]. Furthermore, the IR-absorption signal at 1660 cm^{-1} (which corresponds to the >C=C< vibration of fullerene) increased with the number of addition steps up to the third step in linear or accelerating fashion, for the linear and branched-structure preparation methods, respectively (Figure 6B).

The presence of C_{60} on the electrode surface was also verified electrochemically after each modification step by Cyclic Voltammetry (CV) experiments in 0.1 M Bu_4NPF_6 solutions in CH_2Cl_2 at 288 K in the darkness [23-24]. As expected, the CV response is characterized by a quasi-reversible redox wave for both methods of modification (Fig. 7A - *ii*), the intensity of which should be related to the surface coverage of C_{60}. The CV redox response was confirmed by the direct increase of peak current with increased scan rate (data not shown). Retarded electronic transference was observed with the increasing presence of dendrimers, which are organic molecules that introduce electrical resistance to the interface. Figure 7B shows the charge passed in the C_{60} reduction peaks obtained by CV for both modification methods as functions of the number of C_{60} layers added. In the case of the dendritic films, only a very slight CV response was recorded, with the highest charge obtained at the first step (Fig. 7B ♦), presumably because of the major electronic resistance introduced in the subsequent addition steps that is associated with the blanketing of poorly organized C_{60}-PAMAM-C_{60} over the electrode surface. With thicker films of the branched structure the CV signal disappeared, probably because of the greater disorganization of the films in the dendritic structure, even though there is more fullerene on the surface from the additional modification steps as indicated by the FT-IR data. In contrast, with the linear-structure films, the total charge in the cathodic CV current peak increased up to the third addition step (Fig. 7B •) and decreased only after the fourth step. Probably by the last reaction step there was a loss of organization and perhaps some breaking of the bonding between fullerene and dendrimer with the surface, which is indicated also by the weaker C_{60} FT-IR signal obtained after the fourth addition step.

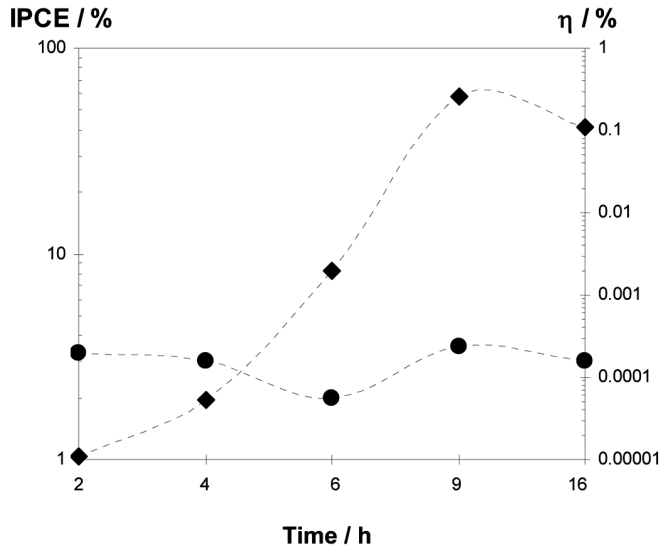

Fig. 5. Values of IPCE % at 430 nm (♦) and h % (•) of modified NSc TiO_2 electrodes silanized with 3% $(CH_3O)_3Si(CH_2)_3NH_2$ as function of the reaction time in a 0.67 mM C_{60} fullerene solution containing 1.33 mM PAMAM G0.0 in 2:1 V/V CH_2Cl_2/toluene at 323K.

Table 1. Photoelectrochemical data for silanized NSc TiO_2 electrodes modified with a mixed solution of (C_{60} – PAMAM G0.0 dendrimer)$_n$ at 298 K, as functions of the modification reaction time.

T/h	IPCE/%	I_{SC}/mA cm^{-2}	V_{OC}/Volts	*ff*	h/%
2	1.05	0.011	0.034	0.225	0.00020
4	1.95	0.011	0.038	0.168	0.00016
6	8.33	0.013	0.007	0.255	0.00005
9	58.28	0.027	0.037	0.100	0.00024
16	40.94	0.019	0.033	0.111	0.00016

Direct electrochemical quantification of the covalently bound fullerene coverage was difficult with these data because of the quasi-reversible character of the CV response. Therefore, UV-Vis spectroscopy was used, taking advantage of the transparent character of the NSc TiO_2 modified electrodes. The spectroscopic signals of fullerene in solution were observed around 340 nm, while the signals observed between 400 to 800 nm for both modification methods (Fig. 8) correspond to the absorption of the -C-N- bond between fullerene and dendrimer [25] and to the signal of the conjugate dienes of fullerene [26]. From the two geometrical structures anticipated in Figure 1, we can estimate the additional UV-Vis absorbance that should be produced by each dendrimer-fullerene addition step. For the linear structure each addition should produce one more layer of fullerene, with the absorbance increasing linearly with the number of addition

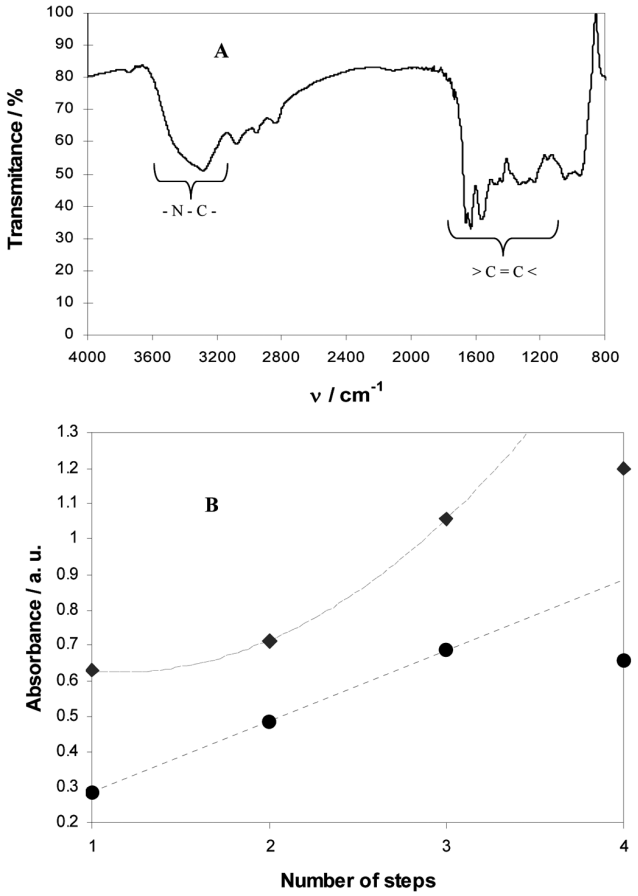

Fig. 6. (**A**) Representative FT-IR Spectra of silanized NSc TiO_2 modified with C_{60}-PAMAM, using as reference the spectrum of silanized NSc TiO_2. (**B**) Comparison of the FT-IR intensities at 1660 cm^{-1} of (•) the linear and (♦) the branched fullerene-dendrimer films as a function of the number of addition steps, using the NSc TiO_2 spectrum as reference.

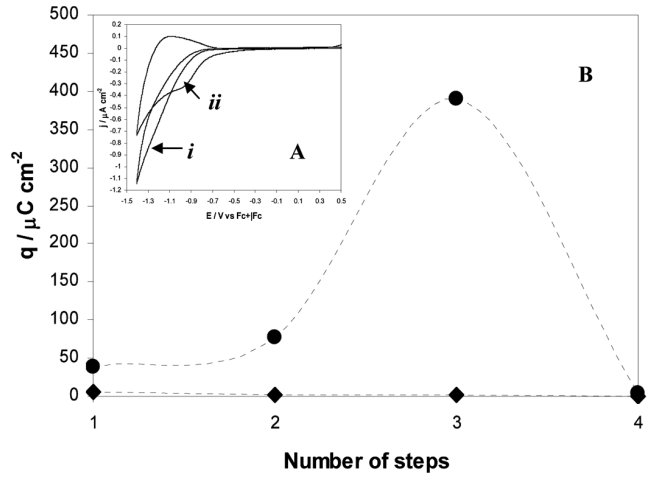

Fig. 7. (**A**) Cyclic voltammograms taken in 0.1M Bu_4NPF_6-CH_2Cl_2 solution at 100 mV s^{-1} and 288 K in darkness, for (***i***) the NSc TiO_2 electrode and (***ii***) silanized NSc TiO_2 modified with one layer of fullerene. (**B**) Comparison of the charge of the cathodic CV current peak with the (•) linear and (♦) branched fullerene-dendrimer films, as a function of the number of fullerene-addition steps.

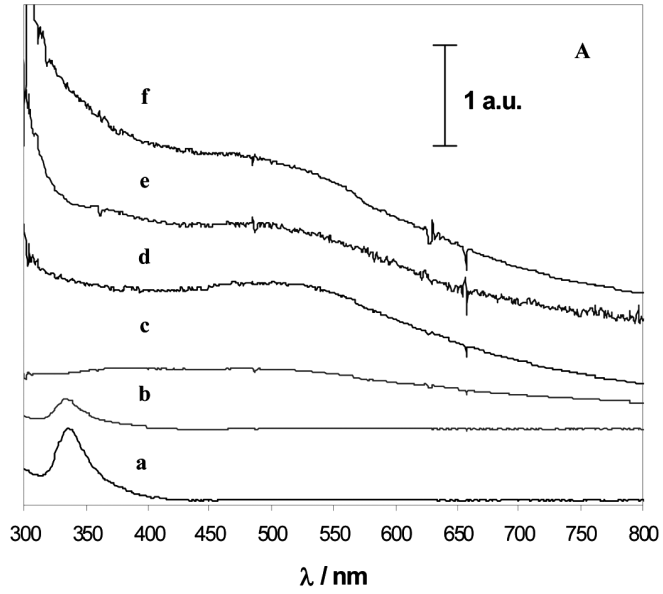

Fig. 8. UV-Visible spectra of (**a**) 4mM C_{60} solution and (**b**) 12mM dendrimer–4mM fullerene solution in 2:1 v/v CH_2Cl_2/toluene. Also presented are (**c**) the self-assembled fullerene deposited on ITO, (**d**) on the silanized NSc TiO_2, and the dendrimer-C_{60} clusters deposited (**e**) on ITO and (**f**) on the silanized NSc TiO_2. The spectra of ITO and of the silanized NSc TiO_2 were used as references for the corresponding fullerene cases.

steps. Figure 9A shows the experimental result for this case, which falls close to the linear relation predicted by assuming one-dimensional growth. Figure 9B shows the data for the branched structure compared with a computed curve based on geometrical branching. It is seen that the actual increase in absorbance, although it is accelerating with each addition step, does not rise as rapidly as the computed curve. Presumably, there is some hindering of the branched additions by the proximity of adjacent structures.

The coverage of the surfaces by fullerene may be estimated from the absorbance data, at least for the linear structure, which should form more or less planar layers. From absorbance measurements of dendrimer-fullerene solutions in 2:1 V/V CH_2Cl_2 /toluene. Bonhôte and co-workers [27] have estimated the extinction coefficient ε of this bond at λ = 594 nm to be 2678 $M^{-1}cm^{-1}$. This value can be used to estimate the number of fullerene groups on the surface, i.e., 4.39×10^{-10}, 7.65×10^{-10}, 1.28×10^{-9} y 1.65×10^{-9} mol cm^{-2}. The resulting value may be used to estimate the fractional coverage of the surface by each layer. Taking the diameter of fullerene to be 7 Å [28], the value of surface coverage by a perfect monolayer of fullerene should be 3.4×10^{-10} mol cm^{-2}. Thus, the agreement with the surface coverage estimated from the incremental change in absorbance shown in Figure 9A for 1, 2, 3 and 4 layers of fullerene added by the linear method [29] indicates that these films achieve full coverage of the surface.

The morphology of the organic films on TiO_2 was studied with SEM and EDX microscopy [30] (Fig. 10). An electrode

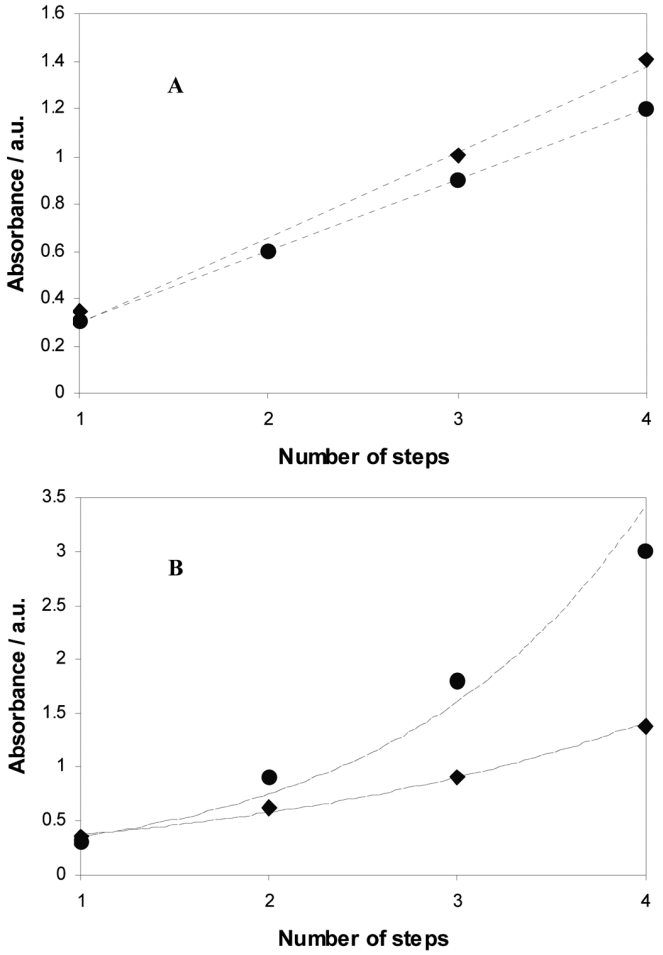

Fig. 9. Computed (•) and experimental (♦) absorbance of C_{60} for the (**A**) linear and (**B**) branched fullerene-dendrimer films, as a function of the number of fullerene-addition steps, obtained at 594 nm.

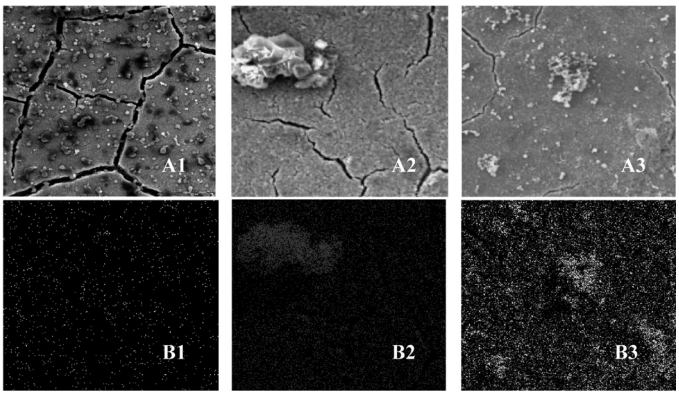

Fig. 10. (**A**) SEM micrographs taken at 2 000X and (**B**) EDX mapping of carbon, taken between 0.19 to 0.29 keV, of silanized NSc TiO_2 surfaces modified with C_{60} – PAMAM G0.0 dendrimers by (**1**) one step in the mixed dendrimer-fullerene solution for 9h, (**2**) one step by the dendritic method, and (**3**) three steps in the linear preparation method.

modified by self assembly of fullerene in the presence of dendrimer during 9 h of reflux presented a more dispersed distribution of carbon composites and in lesser amount (Fig. 10A1 and 10B1) than did the linear and dendritic forms tethered by the silanes. In the cases of both branched and linear films, there were present aggregates of major size (Fig. 10A2 and 10A3, respectively), with a better distribution of material in the elemental mapping experiments (Fig. 10B2 and 10B3, respectively). In the case of the dendritic films, after all steps there were present aggregates such as those in Fig. 10A2, with free space developing between aggregates (Fig. 10B2), which was also evident in the loss of electronic conductance appearing in the CV results. In contrast, with the linear-structure preparation method, the concentration of carbon increased with the number of layers up to the third layer (Fig. 10B3); with the fourth layer, there was accumulation of carbon in certain areas of the electrode indicating some loss of binding between fullerene and dendrimer and limited carbon concentration, as was also evident in the FT-IR results and indicated by the decreased electronic transference in the CV tests. These results demonstrate that the nanoassembled electrodes modified with linear C_{60} fullerene– PAMAM G0.0 dendrimer structures exhibit a better organized interface to provide superior electronic transference by means of the favorable distribution and morphology of the thin conducting fullerene-dendrimer films. On the other hand, it appears that the organized structure begins to degrade during the fourth addition step.

Figure 11 presents the Incident-Photon-to-Current-Conversion-Efficiency (IPCE) at 430 nm of the fullerene films. Figures 12 and 13 show discharge curves of photoelectrochemical cells assembled with iodide solution and the silanized NSc TiO_2 electrodes prepared by the dendritic and linear modification methods, respectively. As seen in Table 2, the dendritic method showed its highest photoconversion efficiency in the first step with IPCE of 8 % and η of 0.00117 %

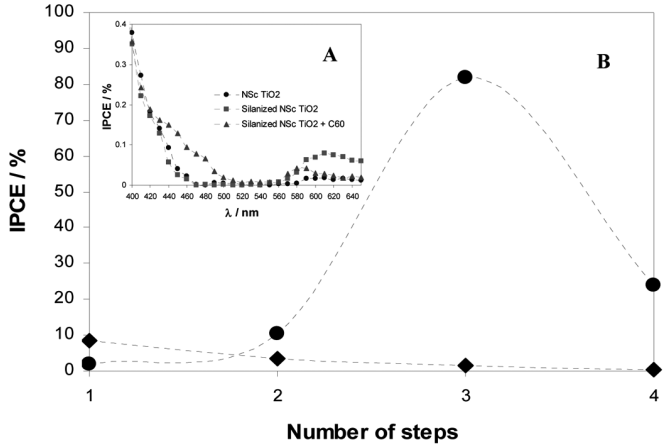

Fig. 11. (**A**) Representative photocurrent-activity spectrum of NSc TiO_2, silanized NSc TiO_2 and silanized NSc TiO_2 + one C_{60} layer constructed by the linear-preparation method. (**B**) Comparison of IPCE % at 430 nm of the (•) linear and (♦) dendritic fullerene-addition methods as a function of the number of addition steps.

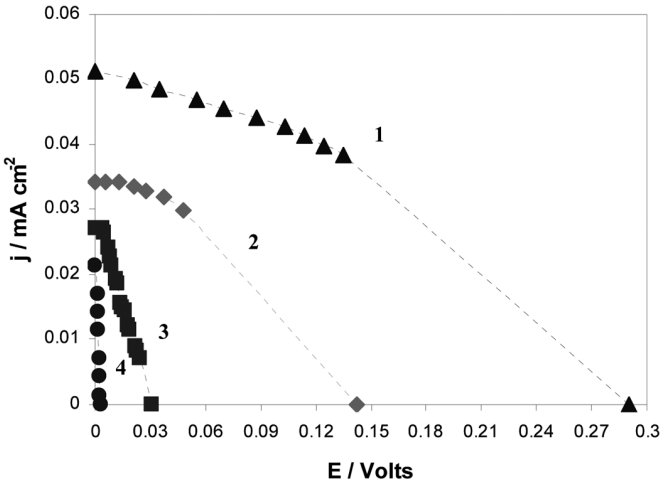

Fig. 12. Photovoltaic discharge curves of the silanized NSc TiO_2 electrode modified with 1, 2, 3 and 4 steps of fullerene addition by the dendritic modification method, taken at 298 K.

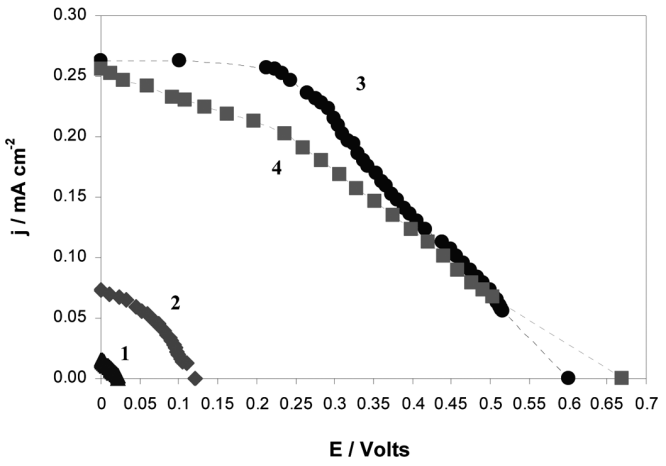

Fig. 13. Photovoltaic discharge curves of the silanized NSc TiO_2 electrode modified with **1, 2, 3** and **4** steps of fullerene by the linear modification method, taken at 298 K.

(Fig. 11♦ and 12, respectively). This value decreased with increased addition steps, presumably as a consequence of the poor organization of the film and the recombination reaction of iodine in the free space within the dendritic composite structure, the porosity of which was seen in the SEM image and the EDX mapping (Fig. 10A2 and 10B2) and indicated also by the CV data (Fig. 7♦). In contrast, in the case of the linear multilayer method, the photoconversion increased layer by layer with the highest IPCE value obtained with three layers of fullerene, 82 % IPCE (Fig. 11 and Table 2) [29]. These values were produced by the high concentration and good organization of the linear fullerene-dendrimer structures, which favor good electronic transference as indicated by the

Table 2. Photoelectrochemical data for silanized NSc TiO_2 electrodes modified with $(C_{60}$ – PAMAM G0.0 dendrimer$)_n$ at 298 K by the dendritic and linear sequential addition methods according to the number of fullerene addition steps.

	IPCE/%	I_{SC}/mA cm^{-2}	V_{OC}/Volts	*ff*	h/%
		Dendritic Method			
1 step	8.34	0.051	0.290	0.333	0.00117
2 step	3.59	0.034	0.142	0.231	0.00026
3 step	1.51	0.027	0.031	0.129	0.00003
4 step	0.30	0.021	0.003	0.424	0.00001
		Linear Method			
1 step	1.84	0.015	0.022	0.311	0.00024
2 step	10.24	0.073	0.120	0.371	0.00764
3 step	81.97	0.263	0.600	0.365	0.13514
4 step	23.97	0.256	0.670	0.275	0.11081

FT-IR, CV, SEM and EDX experiments (Fig. 6·, 7·, 10A3 and 10B3, respectively). Table 2 also presents values for the energy conversion efficiency η, which were obtained by integrating the discharge curves in Figs. 12 and 13 to obtain the electrical power output and dividing those values by the optical energy flux. The maximum values of η obtained for the two preparation methods were 0.0012% for one layer in the branched method and 0.135% for three layers of the linear structure.

Finally, since the flat-band potential of TiO_2 electrodes was estimated using the methodology previously reported by Bisquert and co-workers [13, 31], who extended the Mott-Schottky theory to analysis of nanoporous TiO_2 films deposited on ITO plates. With the value of –0.2 V for the TiO_2 the photo-induced charge transfer potential from the excited sensitizer, at E (C_{60}^*/C_{60}^-) = - 0.23V, provides a favorable photocurrent generation process at 430 nm. The superior performance of the films with the linear structure is the consequence of the coordinated charge-transfer processes that contribute to the enhancement of the photocurrent generation by the silanized NSc TiO_2 modified with films of linear C_{60} fullerene–PAMAM G0.0 dendrimer structures as outlined in Figure 14. This Figure illustrates the energetics of the system; aside the estimated flat-band potential of TiO_2, the other energy values were obtained from the literature [3-4, 6].

In summary, the construction of more efficient nanoassembled multilayer films of fullerene C_{60} – PAMAM G0.0 dendrimer composites over silanized NSc TiO_2 electrodes is achieved using a layer-by-layer technique with a linear sequence than with a dendritic or branched structure. The former increases the electronic transference and photocurrent efficiency with three layers of fullerene by enhancing the photon collection while decreasing the recombination effect by virtue of the greater homogeneity and organization of the film on the semiconductor surface.

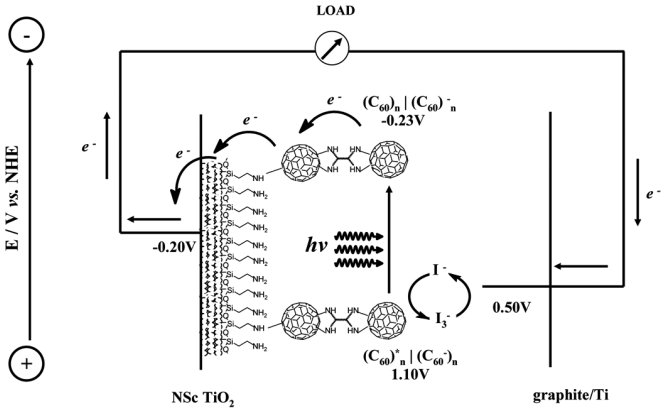

Fig. 14. Energy levels of various redox couples responsible for the charge-transfer processes in the fullerene-dendrimer photoelectrochemical cell.

Experimental

(SnO_2)In conducting glass electrodes (Indium Tin Oxide, ITO) were obtained from Delta Technologies. TiO_2 powder was Degussa P-35 (75% anatase and 25% rutile with 25 nm diameter). $(CH_3O)_3Si(CH_2)_3NH_2$ silane and PAMAM™ Generation 0.0 dendrimers (bearing 4-NH_2 terminal functional groups) were acquired from Aldrich. C_{60} fullerene was provided by Clemson University. Toluene, CH_2Cl_2 and Bu_4NHF_6 were obtained of J. T. Baker and used without further purification.

NSc TiO_2 electrodes were prepared by applying a 4 V potential difference between a steel sheet and the ITO conducting glass substrate immersed in 10 mL of a colloidal suspension (0.5 g TiO_2 in 5 % 2 - propanol in water (V/V)) for 60 s. Following previous reports in the literature [12], the electrodes were then removed from the electrophoretic apparatus, sintered at 723 K in air for 30 min. The NSc TiO_2 electrodes were then exposed to 5 % HCl solutions for 15 min with gentle stirring, rinsed with EtOH for 60 s, and further silanized by exposing the substrates to the corresponding silane. After this chemical treatment, the electrodes were rinsed with EtOH and placed in an oven at 388 K for 15 min to promote the crosslinking of polysiloxane [15].

The electrochemical experiments reported in this work were performed using a PCI4/300™ Potentiostat/Galvanostat/ZRA controlled with Gamry Instruments software, version 4.10© 2002, that was installed in a Pentium based PC. The cyclic voltammetry (CV) experiments were performed at 288 K in darkness in a 10 mL cell equipped with a (SnO_2)In bead, platinum wire and Ag wire as working, counter and pseudo-reference electrode, respectively. Before the CV experiments were carried out, the electrolytic solutions were de-oxygenated by bubbling ultra-pure nitrogen (PRAXAIR, grade 5.0) for at least ten minutes.

The flat-band potential of the nanocrystalline TiO_2 films was obtained by means of Mott-Schottky analysis that involves measurements of differential capacitance in darkness using an IM6 BAS-Zahner potentiostat [13]. Because the TiO_2 layers are highly porous, the treatment of the electrochemical data was done according to the methods reported previously by Bisquert and co-workers [31].

FT-IR spectra were obtained at a 45° reflection angle [8-9] by the specular reflectance technique using Thermo Spectra Tech Equipment and the PVAI-ATR-IR technique. All spectra were obtained with 250 scans at 298 K.

UV-Vis spectra were acquired at 298 K using an Agilent Mod. 8453 UV-Vis spectrophotometer with diode array with two-nanometer resolution and a wavelength range from 190 to 1100 nm. Less than 0.03% stray light was standard.

XRD spectra were taken with Bruker AXS Advanced X-Ray Solutions equipment with 10 scans and step size of 0.2°, rotating the sample at 298 K.

EDX and SEM experiments were made with a JEOL JSM-5400LV Scanning Microscope at 14 kV of acceleration voltage and 90 mA current with 100 s of acquisition time at each augmentation of the images. In the case of the mapping technique, images were obtained at 14 kV of acceleration voltage, applying the energy of each element of interest (C = 0.19 – 0.29 keV; Si = 1.69 – 1.77 keV; Ti = 4.39 – 4.63 keV).

Photocurrent action spectra were obtained for each electrode using a photoelectrochemical cell, which was constructed using the modified electrodes with C_{60} fullerene – PAMAM G0.0 dendrimer films as a photoanode. A Ti substrate covered with a film of colloidal graphite was the counter electrode. A de-oxygenated aqueous solution of 0.3 M KI + 0.015 M I_2 [32] was used with Teflon tape inserted to maintain a 0.5 mm gap between the two electrodes. The following reactions occur in the solar cell when the excited C_{60} interacts with I- to produce C_{60} anions in three steps [12, 33-34]:

(I) $(C_{60})n + h\nu \rightarrow (C_{60})n^*$

(II) $2\,(C_{60})n^* + 3\,I^- \rightarrow 2\,(C_{60})_n^- + I_3^-$

(III) $(C_{60})n^- + (SnO_2)In \mid TiO_2 \rightarrow (C_{60})n + (SnO_2)\,In \mid TiO_2\,(e^-)$

The C_{60}^- anions formed are relatively long-lived and deliver charge to the collecting electrode surface, thereby producing an anodic photocurrent. The undesirable recombination reaction in this system it is

(IV) $(SnO_2)\,In \mid TiO_2\,(2e^-) + I_3^- \rightarrow (SnO_2)In \mid TiO_2 + 3I^-$

IPCE measurements were performed using a IM6 BAS-Zahner Potentiostat, which kept the photo-cells under short circuit conditions, a 100 W Xe lamp Model 6257, and a Model 77250 monochromator (both from Thermo Oriel) [35]. This arrangement was calibrated using an Eppley 17043 Thermopile. The IPCE values were calculated by normalizing the photocurrent values for incident light energy and intensity using the relation [34, 36]: IPCE / % = $(100\% \times 1240 \times I_{SC}) / (I_{inc} \times l)$, where I_{SC} is the short circuit photocurrent density (A cm-2), l is the wavelength (nm) and I_{inc} is the incident light intensity (W cm^{-2}).

Photo-current density vs. voltage (j-V) discharge curves were measured [34] using a variable resistance, 52 kW maximum, as a variable load while the cell was illuminated by a 42.5 mW cm^{-2} (400–800 nm) tungsten-halogen lamp (12V 50W GE) equipped with an integral parabolic reflector and a UV-IR blocking filter. The lamp intensity was calibrated using Alter's air-mass simulator at AM 1.5 [35]. The energy conversion efficiency η was calculated by the relation [4, 36-37]: $h = (jV)_{max} / W_{in}$ where j and V are the current density and potential in the discharge curves (Figs. 12 and 13) and W_{in} is the power flux from lamp illumination (watt-cm^{-2}).

Acknowledgements

The authors acknowledge funding from the Mexican Council for Science and Technology (CONACyT, grant 45157). LE thanks the US National Science Foundation, CHE-0135786, for generous financial support. EB and JM are also grateful to CONACyT for their graduate fellowship. TWC is a CONACyT Cooperante in CIDETEQ under the sponsorship of the US Peace Corps.

References

1. Yan, S. G.; Lyon, L. A.; Lemon, B. I.; Preiskorn, J. S.; Hupp, J. T. *J. Chem. Educ.* **1997**, *6*, 657-662.
2. Grätzel, M. *Solar Energy Materials*, Springer-Verlag Ed., New York, **1982**.
3. O'Regan, B.; Grätzel, M. *Nature* **1991**, *353*, 737-739.
4. Kamat, P. V.; Barazzouk, S.; Tomas, K. G.; Hotchandani, S. *J. Phys. Chem. B* **2000**, *104*, 4014-4017.
5. McEvoy, A. J.; Nazeeruddin, M. K.; Rothenberger, G.; Grätzel, M. *Electrochem. Soc. Proc.* **2001**, *10*, 69.
6. Kamat, P. V.; Barazzouk, S.; Thomas, K. G.; Hotchandani, S. *Electrochem. Soc. Proc.* **2000**, *10*, 62.
7. Peticolas, L. J.; Bean, J. C. *J. Am. Chem. Soc.* **1993**, *115*, 4383-4384.
8. Caldwell, W. B.; Chen, K.; Mirkin, C. A.; Babinec, S. J. *Langmuir* **1993**, *9*, 1945-1947.
9. Li, D.; Swanson, B. I. *Langmuir,* **1993**, *9*, 3341-3344.
10. Chen, K.; Caldwell, W. B.; Mirkin, C. A. *J. Am. Chem. Soc.* **1993**, *115*, 1193-1194.
11. Fröehling, P. E. *Dyes Pigments* **2001** *48*, 187-195.
12. Smeatad, G. P.; Grätzel, M. *J. Chem. Educ.* **1998**, *75*, 752-756.
13. Manríquez, J.; Godínez, L. A. *Thin Solid Films* **2007**, *515*, 3402-3413.
14. Pelouchova, H.; Janda, P.; Weber, J.; Kavan, L. *J. Electroanal. Chem.* **2004**, *566*, 73-83.
15. Tong, Q. Y.; Gösele, U. *Semiconductor Wafer Bonding: Science and Technology*, John Wiley & Sons, Inc., New York, **1999**.
16. Netzer, L.; Sagiv, J. *J. Am. Chem. Soc.* **1983**, *105*, 674-676.
17. Brett, C. W., Chen, K.; Mirkin, C. A.; Babinec, S. J. *Langmuir* **1993**, *9*, 1945-1947.
18. Guldi, D. M.; Pellarini, F.; Prato, M.; Ito, C.; Troisi, L. *Nanoletters* **2002**, *9*, 965-968.
19. Plonska, M. E.; Bettencourt-Dias, A.; Balch, A. L.; Winkler, K. *Chem. Mater.* **2003**, *15*, 4122-4131.
20. Kuptsov, A. H.; Zhizhin, G. N. *Handbook of Fourier Transform Raman and Infrared Spectra of Polymers. Physical Sciences Data 45,* Elsevier Ed., The Netherlands, **1998**.
21. Méndez, J.; Page, J. B. *Light Scattering in Solids VIII,* Springer Ed., Berlin, **2000**.
22. Schettino, V.; Pagliai, M.; Ciabini, L.; Cardini, G. *J. Phys. Chem. A* **2001**, *105*, 11192-11196.
23. Arias, F.; Godínez, L. A.; Wilson, S. R.; Kaifer, A. E.; Echegoyen, L. *J. Am. Chem. Soc.* **1996**, *118*, 6086-6087.
24. Lund, H.; Hammerich, O. *Organic Electrochemistry*, 4 ed., Marcel Dekker, Inc., New York, **1991**, p.p. 323-339.
25. West, S. P.; Poon, T.; Anderson, J. L.; West, M. A.; Foote, C. S. *J. Chem. Educ.* **1997**, *74*, 311-312.
26. Creswell, C. J.; Runquist, O.; Campbell, M. M. *Análisis Spectral de Compuestos Orgánicos*, Diana Ed., México, D. F., **1979**, pp. 31-102.
27. Bonhôte, P.; Gogniat, E.; Tingry, S.; Barbé, Vlachopoulos, N.; Lenzmann, F.; Comte, P.; Grätzel, M. *J. Phys. Chem. B.* **1998**, *102*, 1498-1507.
28. Seymour, R. B.; Kauffman, G. B. *J. Chem. Educ.* 1992, **69**, 645.
29. Bustos, E.; Manríquez, J.; Echegoyen, L.; Godínez, L. A. *Chem. Comm.* **2005**, 1613-1615.
30. Hasobe, T.; Imahori, H.; Fukuzumi, S.; Kamat, P. *J. Phys. Chem. B* **2003**, *107*, 12105-12112.
31. Fabregat-Santiago, F.; García-Belmonte, G.; Bisquert, J.; Bogdanoff, P.; Zaban, A. *J. Electrochem. Soc.* **2003**, *150*, E293-E298.
32. Hara, K.; Horiguchi, T.; Kinoshita, T.; Sayama, K.; Arakawa, H. *Sol. Energ. Mat. Sol. C.* **2001**, *70*, 151-161.
33. Kamat, P. V.; Haria, M.; Hotchandani, S. *J. Phys. Chem. B* **2004**, *108*, 5166-5170.
34. Cherepy, N. J.; Smestad, G. P.; Grätzel, M.; Zhang, J. Z. *J. Phys. Chem.* **1997**, *101,* 9342-9357.
35. Khazraji, A. C.; Hotchandani, S.; Das, S.; Kamat, P. V. *J. Phys. Chem. B* **1999**, *103*, 4693-4700.
36. Sudeep, P. K.; Ipe, B. I.; Thomas, K. G.; George, M. V.; Barazzouk, S.; Hotchandani, S.; Kamat, P. V. *Nano. Lett.* **2002**, *2*, 29-35.
37. Kamat, P. V.; Barazzouk, S.; Hotchandani, S.; Thomas, K. G. *Chem. Eur. J.* **2000**, *6*, 3914-3921.